SCIENCE CHINA
Technological Sciences

•Article•

September 2020 Vol.63 No.9: 1808–1823
https://doi.org/10.1007/s11431-019-1531-9

Analytical study on pretensioned bolt-cable combined support of large cross-section tunnel

LUO JiWei, ZHANG DingLi, FANG Qian*, LI Ao, SUN ZhenYu & CAO LiQiang

Key Laboratory for Urban Underground Engineering of the Ministry of Education, Beijing Jiaotong University, Beijing 100044, China

Received November 13, 2019; accepted January 18, 2020; published online May 14, 2020

To study the mechanical responses of large cross-section tunnel reinforced by pretensioned rock bolts and anchor cables, an analytical model is proposed. Considering the interaction between rock mass and bolt-cable support, the strain softening characteristic of rock mass, the elastic-plastic characteristic of bolt-cable support, and the delay effect of installation are considered in the model. To solve the different mechanical cases of tunneling reinforced by bolt-cable support, an analytical approach has been put forward to get the solutions of stress and displacement associated with tunneling. The proposed analytical model is verified by numerical simulation. Moreover, parametric analysis is performed to study the effects of pretension force, cross-section area, length, and supporting density of bolt-cable support on tunnel reinforcement, which can provide references for determining these parameters in tunnel design. Based on the analytical model, a new Ground Response Curve (GRC) considering the reinforcement of bolt-cable support is obtained, which shows the pretension forces and the timely installation are important in bolt-cable support. In addition, the proposed model is applied to the analysis of the Great Wall Station Tunnel, a high-speed railway tunnel with a super large cross-section, which shows that the analytical model of bolt-cable support was a useful tool for preliminary design of large cross-section tunnel.

bolt-cable combined support, analytical model, pretension force, large cross-section tunnel, reinforcement

Citation: Luo J W, Zhang D L, Fang Q, et al. Analytical study on pretensioned bolt-cable combined support of large cross-section tunnel. Sci China Tech Sci, 2020, 63: 1808–1823, https://doi.org/10.1007/s11431-019-1531-9

1 Introduction

In recent years, with the development of underground engineering, the design and construction of large cross-section tunnels have received extensive attention. With the increase of tunnel dimension, the rock mass stress distribution due to tunnel excavation would be more complex, and the deformation control of rock mass would be more difficult, which has brought challenges to the design of tunnel support.

Rock bolt is a useful tool for tunnel construction, which can considerably improve the stability of tunnel surrounding rock [1]. The effective use of rock bolts for underground structure support began in the 1940s in the mining industry [2]. From the 1970s up to today, the rock bolt has been widely applied in tunnel projects [3–5], and a series of studies on rock bolting have been carried out [6–14].

For large cross-section tunnels, attempts have been made to improve the rock bolting technologies, such as the development of long rock bolt, pretensioned rock bolt, and pretensioned anchor cable [15–20]. However, due to the complexity of geological materials and environments [21–25], for tunnels with an even larger size or tunneling in unfavorable geological conditions, the aforementioned rock bolting method cannot satisfy the reinforcement requirements. To cater for this issue, a support system composed of pretensioned rock bolts and anchor cables has been developed in tunnel construction. This combined support was first used for the construction of coal roadways and hydropower

*Corresponding author (email: qfang@bjtu.edu.cn)

station caverns [26,27], then it was adopted in the Wumengshan railway tunnel and some others [28]. The previous studies on the bolt-cable combined support mainly use numerical simulation [29,30], field monitoring [31,32], and model test [33]. Currently, few analytical solutions are suitable to investigate the interaction of the rock bolt, anchor cable, and rock mass in tunnel construction.

In this study, we propose an analytical model of tunnel reinforced by pretensioned bolt-cable support. First, we propose analytical solutions for different mechanical cases of the bolt-cable reinforced tunnel. The rock mass behaves as strain softening material. The rock bolt and anchor cable behave elastic-perfectly plastic. The delay effect of bolt-cable support is considered by stress release method. Secondly, our proposed method is verified by numerical simulation results. Thirdly, parametric analyses are performed to study the pretension force, cross-section area, length, and supporting density of bolt-cable support on the mechanical responses produced by tunneling. In addition, the Ground Response Curve (GRC) considering bolt-cable support is also calculated, which can be used to facilitate the bolt-cable support design in tunneling. Finally, the proposed analytical model is applied to the analysis of the Great Wall Station Tunnel and shows a satisfactory prediction ability in tunnel construction.

2 Modelling of tunnel reinforced by pretensioned bolt-cable support

2.1 General assumptions

To obtain the closed-form analytical solutions, a deep tunnel with a circular cross-section in plane strain condition is assumed in this study. The rock mass is assumed to be homogeneous, isotropy, under far-field hydrostatic stress p_0. The pretensioned rock bolts and anchor cables are distributed uniformly around the tunnel perimeter. As shown in Figure 1, R_0 is the tunnel radius, and p_i represents the internal support pressure on tunnel circumference. Comparing with the passive rock bolt or anchor cable, pretensioned members have better reinforcement effects on rock mass [27]. The pretensioned members consist of three parts: anchored length, free length, and anchor head. The anchored length is firstly fixed in the rock mass by grouting or mechanical anchorage. Then, a tensile force is applied to the free length by hydraulic jack which is attached to the anchor head. Consequently, the rock mass is reinforced by the axial forces of rock bolt and anchor cable at both ends of their free lengths.

The initial anchoring forces of rock bolt and anchor cable are equal to their pretension forces (without considering the loss of pretension forces), which are expressed as F_1^0 and F_2^0, respectively. Considering compatible deformation of the

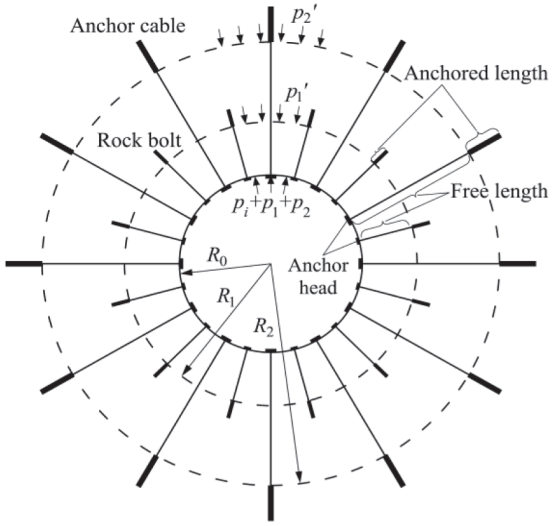

Figure 1 Circular tunnel reinforced by systematic pretensioned rock bolts and anchor cables.

bolt-cable support and the reinforced rock mass, the anchoring forces will increase with the development of rock mass deformation until the rock mass stress and the anchoring forces reach equilibrium. Accordingly, the anchoring forces of rock bolt and anchor cable can be expressed as F_1 and F_2, respectively.

To simplify the analytical model, the uniformly distributed pressures p_1, p_1' and p_2, p_2' are used to substitute for the concentrated forces F_1 and F_2. The p_1' and p_2' are applied at R_1 and R_2, respectively. Their relationships are as follows:

$$\begin{cases} p_1 = \dfrac{F_1}{S_\theta' S_L'} = \lambda_1 F_1, \\ p_2 = \dfrac{F_2}{S_\theta'' S_L''} = \lambda_2 F_2, \end{cases} \tag{1}$$

$$\begin{cases} p_1' = p_1 \dfrac{R_1}{R_0}, \\ p_2' = p_2 \dfrac{R_2}{R_0}, \end{cases} \tag{2}$$

where S_θ' and S_θ'' are the tangential spacings; S_L' and S_L'' are the axial spacings; λ_1 and λ_2 are the supporting densities of rock bolt and anchor cable. The relationship $\lambda = 1/(S_\theta S_L)$ means: for a given value of supporting density λ, the tangential spacing S_θ and axial spacing S_L can be easily derived.

2.2 Delay effect and mechanical behaviors of pretensioned bolt-cable support

In practical engineering, considering the stress release in tunnel excavation, rock mass deformation has been produced before the installation of pretensioned bolt-cable support. It is called the delay effect of installation. If this effect is ne-

glected, the extension lengths of rock bolt and anchor cable will be overestimated, and unreasonable values of F_1 and F_2 will be received. Therefore, the delay effect of the bolt-cable support should be considered in the model [34, 35].

The most popular method to simulate the delay effect of installation is the stress release method [36, 37]. In this paper, it is called the ξ method. According to the moment of installation, this method consists of two stages: In the first stage, the internal pressure ξp_0 is applied to the perimeter of the excavated tunnel, $0<\xi<1$ is the stress release factor. At the same time, the displacement u'_{r} occurs without rock mass reinforcement. In the second stage, rock bolts and anchor cables are installed. The stress ξp_0 is shared by the rock mass and bolt-cable support gradually. In this process, the rock mass stress and the anchoring forces change together with the compatible deformation of the reinforced rock mass and the bolt-cable support until they reach equilibrium. This effect is the interaction between rock mass and bolt-cable support. The relationship between ξ, u'_{r}, u''_{r} is expressed in eq. (3).

$$u_{\mathrm{r}}(\zeta) = u'_{\mathrm{r}}(\zeta) + u''_{\mathrm{r}}(\zeta), \tag{3}$$

where u_{r} is the radial displacement of the rock mass. The value of ξ depends on a series of factors, such as the construction method, rock mass stiffness, plastic model, unreinforced tunnel range, tunnel section area.

It is assumed that rock bolts and anchor cables are axial tension members and elastic-perfectly plastic materials. Figure 2 shows their strain-stress relationship. Then, F_1 and F_2 can be expressed as

$$F_i = \begin{cases} F_i^0 + \varepsilon_{1,i} E_i A_i, & \varepsilon_{1,i} < \varepsilon_{1,i}^p, \\ F_i^p, & \varepsilon_{1,i} \geq \varepsilon_{1,i}^p, \end{cases} \tag{4}$$

where

$$\varepsilon_{1,i} = \frac{\Delta L_i}{L_i} = \frac{u_r''\big|_{r=R_0} - u_r''\big|_{r=R_i}}{L_i},$$

$$\varepsilon_{1,i}^p = \frac{F_i^p - F_i^0}{A_i E_i} = \frac{A_i \sigma_{1,i}^p - F_i^0}{A_i E_i},$$

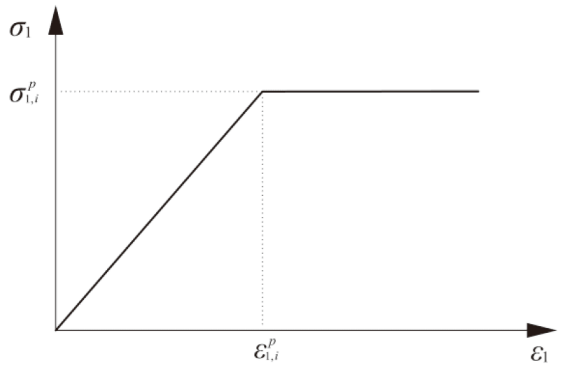

Figure 2 Elastic-perfectly plastic model of rock bolt and anchor cable.

$$i = \begin{cases} 1, & \text{rock bolt}, \\ 2, & \text{anchor cable}, \end{cases}$$

where $\varepsilon_{1,i}$ is axial strain; $\varepsilon_{1,i}^p$ is yield strain; E_i is Young's modulus; A_i is cross-section area; L_i is length; ΔL_i is elongation; F_i^p is yielding force; $\sigma_{1,i}^p$ is yield strength; where the superscript i represents supporting type of the parameter.

2.3 Failure criteria of rock mass

The rock mass is assumed as a strain softening material, as shown in Figure 3. During loading, the rock mass originally behaves linear elastic until the principal stress difference reaches the peak strength. The physical equation of elastic zone can be expressed as

$$\begin{cases} \varepsilon_{\mathrm{r}} = \dfrac{1}{2G}[(1-\nu)(\sigma_{\mathrm{r}} - p_0) - \nu(\sigma_\theta - p_0)], \\ \varepsilon_\theta = \dfrac{1}{2G}[(1-\nu)(\sigma_\theta - p_0) - \nu(\sigma_{\mathrm{r}} - p_0)], \end{cases} \tag{5}$$

where $G = E/[2(1+\nu)]$ is the shear modulus of rock mass; E is Young's modulus; ν is Passion's ratio; σ_θ and σ_{r} are the tangential and radial stress components respectively; ε_θ and ε_{r} are the tangential and radial strain components, respectively.

Then, the rock mass exhibits a strain-softening behavior that its strength reduces with the increase of principal strain. Ultimately the principal stress difference reaches the residual strength, which means the rock mass transit into the plastic residual state. It is assumed that the rock mass follows the Mohr-Coulomb criterion that contains two shear strength parameters, internal friction angle φ, and cohesion c. The general form of Mohr-Coulomb strength criterion in a polar coordinate system is as follows:

$$\sigma_\theta = \alpha\sigma_{\mathrm{r}} + \sigma_{\mathrm{c}}, \tag{6}$$

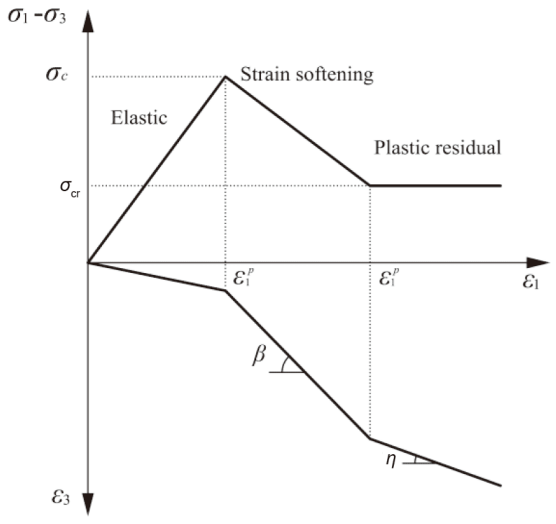

Figure 3 Strain softening constitutive model of rock mass.

where $\alpha = (1+\sin\varphi)/(1-\sin\varphi)$, and $\sigma_c = 2c\cos\varphi/(1-\sin\varphi)$ is the uniaxial compressive strength.

According to a series of laboratory experiments, it is proved that the loss of cohesion is the origin of strength loss throughout the plastic softening state [38, 39]. Moreover, their experiments show that c decreases with the development of plastic strain, while φ is nearly a constant. In the following discussion, for the strain softening behavior of rock mass, the cohesion c is assumed to reduce with the increase of tangential strain, as expressed in eq. (7). Meanwhile, the internal friction angle φ is assumed to be constant.

$$c = c_p - K_c\varepsilon_\theta^p, \tag{7}$$

where K_c is the cohesion softening modulus; c_p is the cohesion at peak strength; ε_θ^p is the tangential plastic strain. Based on eq. (6), the Mohr-Coulomb strength criterion of plastic strain softening state can be expressed as

$$\sigma_\theta = \alpha\sigma_r + \sigma_{cp} - M_c\varepsilon_\theta^p, \tag{8}$$

where $\sigma_{cp} = 2c_p\cos\varphi/(1-\sin\varphi)$ is the peak strength, and $M_c = 2K_c\cos\varphi/(1-\sin\varphi)$ is the softening modulus of rock mass.

When the rock mass developed to the plastic residual state, the strength criterion can be expressed by eq. (9).

$$\sigma_\theta = \alpha\sigma_r + \sigma_{cr}, \tag{9}$$

where

$$\sigma_{cr} = \frac{2c_r\cos\varphi}{1-\sin\varphi},$$

σ_{cr} is the residual strength; c_r is the cohesion of residual state. In this paper, a symmetrical plane strain problem is studied. The equilibrium equation becomes:

$$\frac{\mathrm{d}\sigma_r}{\mathrm{d}r} + \frac{\sigma_r - \sigma_\theta}{r} = 0. \tag{10}$$

The relationship between strain and displacement is as follows:

$$\varepsilon_r = \frac{\mathrm{d}u_r}{\mathrm{d}r}, \tag{11a}$$

$$\varepsilon_\theta = \frac{u_r}{r}, \tag{11b}$$

where u_r is the radial displacement of rock mass.

In strain softening state, the strains are decomposed into elastic and plastic, respectively. And the strains are decomposed into elastic, plastic, and residual in the residual state, as follows:

$$\begin{cases} \varepsilon_r = \varepsilon_r^e + \varepsilon_r^p, \\ \varepsilon_\theta = \varepsilon_\theta^e + \varepsilon_\theta^p, \end{cases} \tag{12}$$

$$\begin{cases} \varepsilon_r = \varepsilon_r^e + \varepsilon_r^p + \varepsilon_r^r, \\ \varepsilon_\theta = \varepsilon_\theta^e + \varepsilon_\theta^p + \varepsilon_\theta^r. \end{cases} \tag{13}$$

The superscripts e, p, and r represent elastic, plastic softening, and residual strains, respectively.

Dilation angle ψ is introduced to describe the dilatancy behavior of rock mass. The non-associated flow rule is adopted to represent the relationship between radial and tangential plastic strain increments, in which the dilation angle ψ is not equal to the friction angle φ. In the strain softening state, the dilation angle is ψ_1, and the plastic potential function is

$$Q = \sigma_\theta - \beta\sigma_r - \sigma_{cp}, \tag{14}$$

where

$$\beta = \frac{1+\sin\psi_1}{1-\sin\psi_1}.$$

The non-associated flow rule of the plastic strain softening zone is

$$\varepsilon_r^p + \beta\varepsilon_\theta^p = 0. \tag{15}$$

According to eqs. (11) and (12), eq. (15) can be written as the following differential equation:

$$\frac{\mathrm{d}u_r}{\mathrm{d}r} + \beta\frac{u_r}{r} = \varepsilon_r^e + \beta\varepsilon_\theta^e. \tag{16}$$

The dilation angle is ψ_2 in the plastic residual state, and the plastic potential function is

$$Q = \sigma_\theta - \eta\sigma_r - \sigma_{cr}, \tag{17}$$

where

$$\eta = \frac{1+\sin\psi_2}{1-\sin\psi_2}.$$

The non-associated flow rule of the plastic residual zone is

$$\varepsilon_r^r + \eta\varepsilon_\theta^r = 0. \tag{18}$$

Then, eq. (18) can be written as

$$\frac{\mathrm{d}u_r}{\mathrm{d}r} + \eta\frac{u_r}{r} = \varepsilon_r^e + \varepsilon_r^p + \eta(\varepsilon_\theta^e + \varepsilon_\theta^p). \tag{19}$$

3 Analytical solutions

According to the constitutive model shown in Figure 3, there are three possible zones of rock mass around the tunnel: elastic, plastic strain softening, and plastic residual. R_p and R_r are used to represent the boundary radii of the three zones.

It is assumed that the original state of rock mass is elasticity. For the stage after tunnel excavation and before the installation of bolt-cable support, stress field varies continuously with stress release. In this stage, the strain softening zone and residual zone may appear according to the stress release magnitude. As shown in Figure 4(a), there are three possible cases of the mechanical state on rock mass around the tunnel. The solutions of these cases can be obtained by the stress release method.

After the installation of rock bolt and anchor cable, the rock mass is reinforced. Referring to the boundary radii R_p and R_r, together with the reinforced radii of rock bolt R_1 and anchor cable R_2, there are nine possible cases required to be

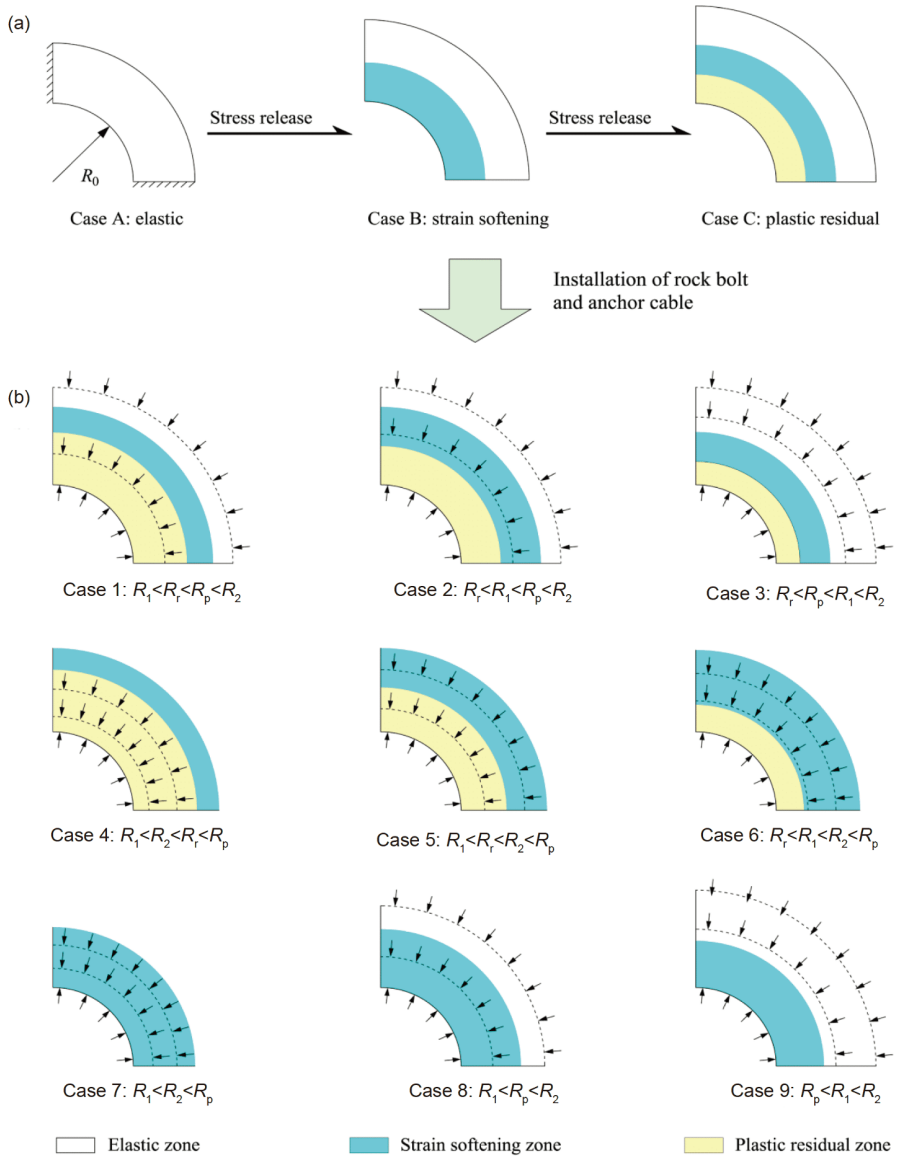

Figure 4 (Color online) Mechanical cases of the tunnel. (a) Before installation of bolt-cable support; (b) after installation of bolt-cable support.

discussed, as shown in Figure 4(b). From Case 1 to Case 6, the elastic, strain softening and plastic residual zones coexist, while the reinforced radii R_1 and R_2 of bolt-cable support are different. From Case 7 to Case 9, only the elastic and strain softening zones exist. In these cases, it is assumed that the bolt-cable support and the rock mass work consistently, and there is no slippage between the bolt-cable support and the rock mass. These cases are interrelated; their transformation from one case to another may occur in the stress release process. For example, Case A→Case B→Case C→Case 3→Case 2 is a possible transformation path in tunneling process. We use Case 2 in the following to illustrate the solution process. The solutions of other cases are shown in the Appendix (https://link.springer.com).

3.1 Solution for Case 2

In Case 2, the cables are anchored in the elastic zone, while the rock bolts are anchored in the strain softening zone. As shown in Figure 4, the relationship of the radii is $R_r<R_1<R_p<R_2$.

3.1.1 *Solution for elastic zone*

(1) $r>R_2$. The rock mass is in elastic state. Its boundary conditions are represented as $\sigma_r=\sigma_r^{R_2}$ at $r=R_2$, and $\sigma_r=p_0$ at $r=\infty$. There are no supporting members in this region, and the stresses are as follows:

$$\sigma_r=p_0-(p_0-\sigma_r^{R_2})\frac{R_2^2}{r^2}, \tag{20a}$$

$$\sigma_\theta = p_0 + (p_0 - \sigma_r^{R_2})\frac{R_2^2}{r^2}. \tag{20b}$$

The rock mass displacement and strains are as follows:

$$u_r = \frac{1}{2G}(p_0 - \sigma_r^{R_2})\frac{R_2^2}{r}, \tag{21}$$

$$\varepsilon_r = \frac{1}{2G}(\sigma_r^{R_2} - p_0)\frac{R_2^2}{r^2}, \tag{22a}$$

$$\varepsilon_\theta = \frac{1}{2G}(p_0 - \sigma_r^{R_2})\frac{R_2^2}{r^2}. \tag{22b}$$

(2) $R_p<r\le R_2$. In this region, the rock mass is in elastic state, which is under the boundary conditions: $\sigma_r^{R_2}+p_2'$ at $r=R_2$ and $\sigma_r^{R_p}$ at $r=R_p$. According to the classical elasticity [40], the stresses are

$$\sigma_r = -B_1\left(\frac{R_p}{r}\right)^2 + C_1, \tag{23a}$$

$$\sigma_\theta = B_1\left(\frac{R_p}{r}\right)^2 + C_1, \tag{23b}$$

where

$$B_1 = \frac{R_2^2\left(\sigma_r^{R_2}+p_2^{'}-\sigma_r^{R_p}\right)}{R_2^2-R_p^2},$$

$$C_1 = \frac{\left(\sigma_r^{R_2}+p_2^{'}\right)R_2^2-\sigma_r^{R_p}R_p^2}{R_2^2-R_p^2}.$$

The solution of displacement and strains are

$$u_r = \frac{r}{2G}\left[B_1\left(\frac{R_p}{r}\right)^2 + (1-2\nu)(C_1-p_0)\right], \tag{24}$$

$$\varepsilon_r = \frac{1}{2G}\left[-B_1\left(\frac{R_p}{r}\right)^2 + (1-2\nu)(C_1-p_0)\right], \tag{25a}$$

$$\varepsilon_\theta = \frac{1}{2G}\left[B_1\left(\frac{R_p}{r}\right)^2 + (1-2\nu)(C_1-p_0)\right]. \tag{25b}$$

In these solutions, $\sigma_r^{R_p}$, $\sigma_r^{R_2}$, R_p and p_2' are the unknown parameters to be solved. Based on the displacement continuity condition at the boundary between the elastic zone and the strain softening zone, the radial stress at $r=R_p$ can be derived.

$$\sigma_r^{R_p} = \frac{1}{\alpha+1}\left(2p_0 + \frac{1}{1-\nu}p_2' - \sigma_{cp}\right). \tag{26}$$

According to the displacement continuity condition at cable anchoring position, the radial stress at $r=R_2$ is obtained as

$$\sigma_r^{R_2} = p_0\left[1-\left(\frac{R_p}{R_2}\right)^2\right] + \sigma_r^{R_p}\left(\frac{R_p}{R_2}\right)^2 - \frac{p_2'}{2(1-\nu)}\left[\left(\frac{R_p}{R_2}\right)^2 + 1 - 2\nu\right]. \tag{27}$$

3.1.2 *Solution for strain softening zone*

In the strain-softening zone, the strains are decomposed into elastic and plastic parts. According to the differential equation eq. (16) and the displacement continuity condition at $r=R_p$. The displacement is

$$u_r = D_1 R_p^{1+\beta} r^{-\beta} + H_1 r, \tag{28}$$

where

$$D_1 = \frac{B_1}{G(\beta+1)},$$

$$H_1 = \frac{1}{2G}\left[\frac{\beta-1}{\beta+1}B_1 + (1-2\nu)(C_1-p_0)\right].$$

Substituting eq. (28) into eq. (11), the strains are solved.

$$\varepsilon_r = -\beta D_1\left(\frac{R_p}{r}\right)^{\beta+1} + H_1, \tag{29a}$$

$$\varepsilon_\theta = D_1\left(\frac{R_p}{r}\right)^{\beta+1} + H_1. \tag{29b}$$

Due to the anchoring position of rock bolts, the strain softening zone is divided into two parts.

(1) $R_1<r\le R_p$. In this region, the stress boundary condition is $\sigma_r|_{r=R_p}$ which has been solved by eq. (26). Based on the strain relationship of eq. (12) together with eqs. (25b) and (29b), the radial and tangential stresses can be obtained by substituting eq. (8) into eq. (10).

$$\sigma_r = N_1\left(\frac{r}{R_p}\right)^{\alpha-1} + D_1 M_c\left[\frac{1}{\alpha+\beta}\left(\frac{R_p}{r}\right)^{1+\beta} - \frac{1}{\alpha-1}\right] - \frac{\sigma_{cp}}{\alpha-1}, \tag{30a}$$

$$\sigma_\theta = \alpha\sigma_r + \sigma_{cp} - D_1 M_c\left[\left(\frac{R_p}{r}\right)^{\beta+1} - 1\right], \tag{30b}$$

where

$$N_1 = \sigma_r^{R_p} + \frac{\sigma_{cp}}{\alpha-1} - D_1 M_c\left(\frac{1}{\alpha+\beta} - \frac{1}{\alpha-1}\right).$$

(2) $R_r\le r<R_1$. In this region, the boundary condition is $\sigma_r = \sigma_r|_{r=R_1} + p_1'$ at $r=R_1$, where $\sigma_r|_{r=R_1}$ is the result of eq. (30a). Consequently, the stresses are obtained as

$$\sigma_r = N_1\left(\frac{r}{R_p}\right)^{\alpha-1} + D_1 M_c\left[\frac{1}{\alpha+\beta}\left(\frac{R_p}{r}\right)^{1+\beta} - \frac{1}{\alpha-1}\right] + p_1'\left(\frac{r}{R_1}\right)^{\alpha-1} - \frac{\sigma_{cp}}{\alpha-1}, \tag{31a}$$

$$\sigma_\theta = \alpha\sigma_r + \sigma_{cp} - D_1 M_c\left[\left(\frac{R_p}{r}\right)^{\beta+1} - 1\right]. \tag{31b}$$

3.1.3 *Solution for plastic residual zone*

Similar to the analysis of the strain softening zone, con-

sidering the displacement continuity condition $u_{\mathrm{r}}|_{\mathrm{r}=R_{\mathrm{r}}}$, the displacement is solved as

$$u_{\mathrm{r}} = D_2 R_{\mathrm{r}}^{\eta+1} r^{-\eta} + H_2 r, \tag{32}$$

where

$$D_2 = \frac{B_1}{G(1+\eta)}\left(\frac{R_{\mathrm{p}}}{R_{\mathrm{r}}}\right)^{\beta+1},$$

$$H_2 = D_2\frac{\eta-\beta}{\beta+1} + H_1.$$

Hence, by substituting eq. (32) into eq. (11), the strains are

$$\varepsilon_{\mathrm{r}} = -\eta D_2\left(\frac{R_{\mathrm{r}}}{r}\right)^{\eta+1} + H_2, \tag{33a}$$

$$\varepsilon_{\theta} = D_2\left(\frac{R_{\mathrm{r}}}{r}\right)^{\eta+1} + H_2. \tag{33b}$$

By substituting eq. (9) into eq. (10) and considering the boundary condition $\sigma_{\mathrm{r}}|_{\mathrm{r}=R_{\mathrm{r}}}$ of eq. (31a), the stresses are

$$\sigma_{\mathrm{r}} = N_1\left(\frac{r}{R_{\mathrm{p}}}\right)^{\alpha-1} + N_2\left(\frac{r}{R_{\mathrm{r}}}\right)^{\alpha-1} + p'_1\left(\frac{r}{R_1}\right)^{\alpha-1} - \frac{\sigma_{\mathrm{cr}}}{\alpha-1}, \tag{34a}$$

$$\sigma_{\theta} = \alpha\sigma_{\mathrm{r}} + \sigma_{\mathrm{cr}}, \tag{34b}$$

where

$$N_2 = \frac{B_1 M_{\mathrm{c}}}{G(\beta+1)}\left[\frac{1}{\alpha+\beta}\left(\frac{R_{\mathrm{p}}}{R_{\mathrm{r}}}\right)^{1+\beta} - \frac{1}{\alpha-1}\right] + \frac{\sigma_{\mathrm{cr}}-\sigma_{\mathrm{cp}}}{\alpha-1}.$$

3.1.4 Radii of strain softening and residual zone

According to the equations obtained above, there are still several unknowns: the strain softening radius R_{p}, the residual radius R_{r}, the pressures p_1 and p_2. Considering the continuous condition of tangential stress σ_{θ} at the softening-residual boundary and using eqs. (26b) and (30b) at $r=R_{\mathrm{b}}$, the residual radius is solved as

$$R_{\mathrm{p}} = R_{\mathrm{r}}\left(\frac{\sigma_{\mathrm{cp}}-\sigma_{\mathrm{cr}}}{M_{\mathrm{c}}D_1}+1\right)^{-\frac{1}{1+\beta}}. \tag{35}$$

Then, the stress condition $\sigma_{\mathrm{r}}|_{\mathrm{r}=R_0} = p_i + p_1 + p_2$ is used to solve R_{p}. As the anchoring forces is closely related to the delay effect, so eqs. (1)–(4) are used to solve p_1 and p_2. In eq. (3), the rock mass displacement u_{r}' before installation is carried out by the ξ method in the following section.

3.2 Rock mass displacement before installation of bolt-cable support

The delay effect of installation can be evaluated by the ξ method. It is a stress release method that the rock mass deformation is calculated by applying an internal pressure ξp_0 to the perimeter of the excavated tunnel. Before the installation of bolt-cable support, the possible mechanical states are expressed as Cases A–C in Figure 4(a).

3.2.1 Solution for Case C

It is easy to know that Case C is similar to Cases 1–6, but there is no anchoring force in Case C. So, by substituting $p_1 = p_1' = p_2 = p_2' = 0$ and $p_i = \zeta p_0$ into the solution of Case 2 (or other cases in Cases 1–6 in the Appendix), the solution of Case C is easily derived. This method can get all the stress, strain, and displacement solutions. Due to length constraints, only the displacement solutions are given in this paper, as follows:

$$u_{\mathrm{r}} = \begin{cases} 1/2G(p_0 - \sigma_r^{R_{\mathrm{p}}})R_{\mathrm{p}}^2/r, & r \geq R_{\mathrm{p}}, \\ D_5 R_{\mathrm{p}}^{1+\beta} r^{-\beta} + H_5 r, & R_{\mathrm{r}} \leq r < R_{\mathrm{p}}, \\ D_6 R_{\mathrm{r}}^{1+\eta} r^{-\eta} + H_6 r, & R_0 \leq r < R_{\mathrm{r}}, \end{cases} \tag{36}$$

where

$$\sigma_r^{R_{\mathrm{p}}} = p_0(1-\sin\varphi) - c_{\mathrm{p}}\cos\varphi,$$

$$D_5 = \frac{p_0\sin\varphi + c_{\mathrm{p}}\cos\varphi}{G(1+\beta)},$$

$$D_6 = \frac{(p_0\sin\varphi + c_{\mathrm{p}}\cos\varphi)}{G(1+\eta)}\left(\frac{R_{\mathrm{p}}}{R_{\mathrm{r}}}\right)^{1+\beta},$$

$$H_5 = \frac{(p_0\sin\varphi + c_{\mathrm{p}}\cos\varphi)(\beta-1)}{2G(\beta+1)},$$

$$H_6 = \frac{1}{2G}\left(p_0\sin\varphi + c_{\mathrm{p}}\cos\varphi\right) \times\left[\left(\frac{R_{\mathrm{p}}}{R_{\mathrm{r}}}\right)^{1+\beta}\left(\frac{2}{1+\beta} - \frac{2}{1+\eta}\right) + \frac{\beta-1}{\beta+1}\right].$$

According to the continuity condition of tangential stress σ_{θ} at the softening-residual boundary and radial stress condition $\sigma_{\mathrm{r}}|_{\mathrm{r}=R_0} = \zeta p_0$ at the tunnel circumference, the boundary radii are

$$R_{\mathrm{p}} = R_{\mathrm{r}}\left[\frac{\sigma_{\mathrm{cp}}-\sigma_{\mathrm{cr}}}{M_{\mathrm{c}}D_5}+1\right]^{-\frac{1}{1+\beta}}, \tag{37}$$

$$R_{\mathrm{r}} = R_0\left[N_5\left(\frac{\sigma_{\mathrm{cp}}-\sigma_{\mathrm{cr}}}{M_{\mathrm{c}}D_5}+1\right)^{-\frac{\alpha-1}{1+\beta}} + J_1\right]^{\frac{1}{\alpha-1}} \times\left[\zeta p_0 + \frac{\sigma_{\mathrm{cr}}}{\alpha-1}\right]^{-\frac{1}{\alpha-1}}, \tag{38}$$

where

$$N_5 = \sigma_r^{R_{\mathrm{p}}} + \frac{\sigma_{\mathrm{cp}}}{\alpha-1} - M_{\mathrm{c}}D_5\left(\frac{1}{\alpha+\beta} - \frac{1}{\alpha-1}\right),$$

$$J_1 = \left(M_{\mathrm{c}}D_5 + \sigma_{\mathrm{cp}} - \sigma_{\mathrm{cr}}\right)\left(\frac{1}{\alpha+\beta} - \frac{1}{\alpha-1}\right).$$

The appearance of the plastic residual state along tunnel circumference is the application condition of Case C. So,

substituting $R_r=R_0$ into the radial stress equation of the plastic residual zone. The application condition of Case C is solved as eq. (39).

$$\zeta p_0 < N_5\left(\frac{\sigma_{cp}-\sigma_{cr}}{M_c D_5}+1\right)^{\frac{1-\alpha}{1+\beta}}+J_2, \tag{39}$$

where

$$J_2 = M_c D_5\left[\frac{1}{\alpha+\beta}\left(\frac{\sigma_{cp}-\sigma_{cr}}{M_c D_5}+1\right)-\frac{1}{\alpha-1}\right] - \frac{\sigma_{cp}}{\alpha-1}.$$

3.2.2 *Solutions for Cases A and B*

The solution of Case C can degenerate to the corresponding ones of Cases A and B.

(1) Case A. For Case A, all the rock mass is in elastic state, and the radial displacement is

$$u_r = \frac{1}{2G}(p_0-\zeta p_0)\frac{R_0^2}{r}, \tag{40}$$

where $\zeta p_0 \geq p_0(1-\sin\varphi)-c_p\cos\varphi$ is the application condition of Case A.

(2) Case B. In this case, rock mass near the tunnel circumference begins to show the strain softening behavior. Then, the rock mass displacement is

$$u_r = \begin{cases} 1/2G(p_0-\sigma_r^{R_p})R_p^{\,2}/r, & r>R_p, \\ D_5 R_p^{\,1+\beta} r^{-\beta}+H_5 r, & R_0<r<R_p, \end{cases} \tag{41}$$

where $\sigma_r^{R_p}$ is the same as eq. (36). The radial stress at the strain softening zone ($R_0 \leq r < R_p$) is

$$\sigma_r = N_5\left(\frac{r}{R_p}\right)^{\alpha-1}+M_c D_5\left[\frac{1}{\alpha+\beta}\left(\frac{R_p}{r}\right)^{1+\beta}-\frac{1}{\alpha-1}\right] - \frac{\sigma_{cp}}{\alpha-1}. \tag{42}$$

Considering the radial stress condition $\sigma_r|_{r=R_0}=\zeta p_0$, R_p can be solved. The application condition of Case B is

$$N_5\left(\frac{\sigma_{cp}-\sigma_{cr}}{M_c D_5}+1\right)^{\frac{1-\alpha}{1+\beta}}+J_2 \leq \zeta p_0 < p_0(1-\sin\varphi)-c_p\cos\varphi. \tag{43}$$

4 Verification

To verify our proposed analytical solutions, the results of the analytical model are compared with those obtained from the numerical simulation. The numerical simulation is performed using a 3D finite difference code FLAC3D. In the FLAC3D software, the cable structural elements (cableSELs), which are two noded and straight finite elements, can yield in tension or compression. The rock bolt and anchor cable can be modeled as collections of cableSELs. The anchor heads and anchor lengths of the bolt-cable support can be connected to the rock mass zones by rigid links. A quarter of the geometry is modeled due to symmetry. Figure 5 shows the geometry of the mesh. The height, width, and thickness of the model are 160, 160, and 2.4 m, respectively. The radius of the circular tunnel is 12 m. The mechanical parameters of rock mass, bolts, and cables are listed in Table 1, which are based on the engineering design data and geological investigation data of the Great Wall Station Tunnel project (a high-speed large cross-section railway tunnel in weak rock mass).

According to our analytical model, the radii of the plastic strain softening zone R_p=21.0 m and residual zone R_r=15.9 m can be derived by substituting the mechanical parameters into the analytical solutions. The relationship of $R_r<R_1<R_p<R_2$ can be obtained, which means the mechanical state can be solved by Case 2.

The anchoring forces obtained by our analytical method and numerical simulation are shown in Figure 6. The analytical results agree well with the numerical simulation results. As shown in Figure 7, our analytical results of tunnel radial displacement are consistent with those of the numerical simulation. The value of u_r from the numerical simulation is smaller than that from the analytical method, then the two curves tend to be closer with the increase of r. The stress distributions are shown in Figure 8. The tangential stress σ_θ increases rapidly in the plastic zone until reaching peak stress at the elastic-plastic boundary. Then, it gradually decreases in the elastic zone and eventually tends to be stable at the stress p_0. The plastic radii R_p, which can be calculated by the location of the peak tangential stress, obtained by the two methods are close. With the increase of the distance to the tunnel opening, the radial stress σ_r gradually increases and tends to be stable at p_0. According to the consistency of the

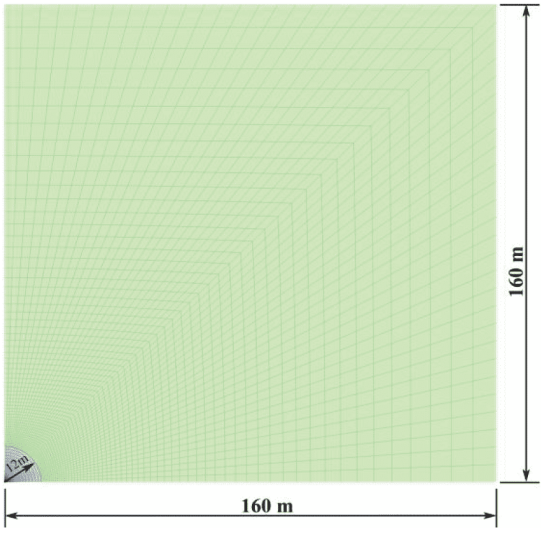

Figure 5 (Color online) Numerical simulation model by FLAC3D.

Table 1 Mechanical parameters of rock mass, rock bolt, and anchor cable

Parameter	Value
Tunnel radius R_0	12 m
Far-field hydrostatic stress p_0	2.80 MPa
Uniaxial compressive strength of rock mass σ_{cp}	1.33 MPa
Residual strength of rock mass σ_{cr}	0.33 MPa
Poisson's ratio of rock mass v	0.33
Shear modulus of rock mass G	700 MPa
Softening modulus of rock mass M_c	300 MPa
Stress release factor ξ	0.10
Cross-section area of rock bolt A_1	490 mm^2
Rock bolt length L_1	7 m
Pretension force of rock bolt F_1^0	120 kN
Yielding force of rock bolt F_1^P	205 kN
Supporting density of rock bolt λ_1	0.69
Young's modulus of rock bolt E_1	195 GPa
Cross-section area of anchor cable A_2	840 mm^2
Anchor cable length L_2	14 m
Pretension force of anchor cable F_2^0	850 kN
Yielding force of anchor cable F_2^P	1326 kN
Supporting density of anchor cable λ_2	0.13
Young's modulus of anchor cable E_2	195 GPa

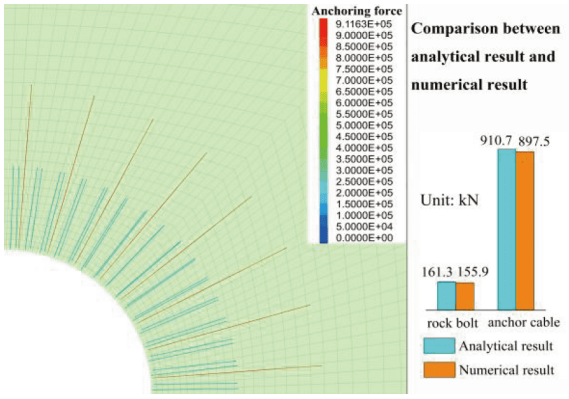

Figure 6 Anchoring forces of rock bolts and anchor cables.

stress curves between the numerical and the analytical results, our proposed analytical solutions are verified.

5 Analysis of pretensioned bolt-cable support in tunnel reinforcement

5.1 Anchoring forces and rock mass displacement

The anchoring force is composed of two parts: one part is the pretension force, and the other part is the passive anchoring force caused by compatible deformation of the reinforced rock mass and the bolt-cable support. Hence, the anchoring

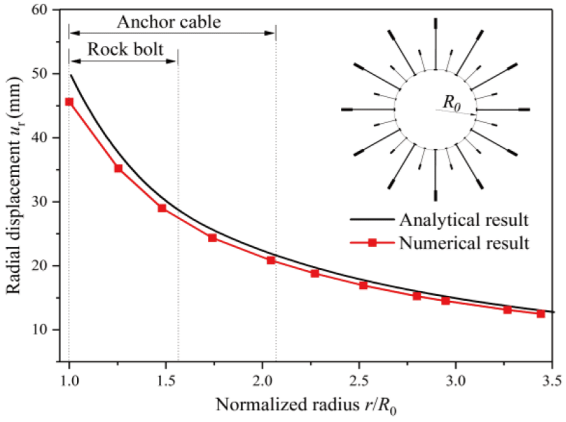

Figure 7 Comparison of radial displacement of rock mass.

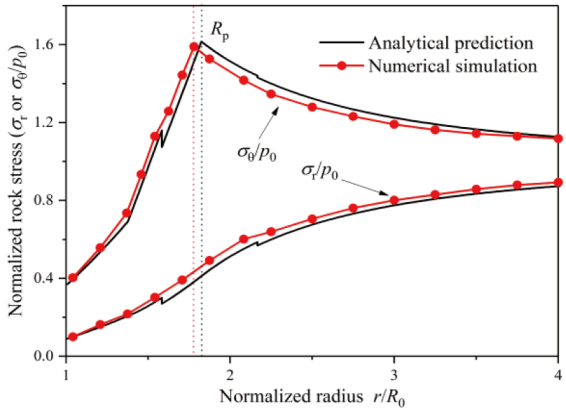

Figure 8 Comparison of stress distribution of rock mass.

forces F_1 and F_2, which represent the mechanical state (elastic or yielding) of rock bolt and anchor cable, are determined by the parameters of bolt-cable support. In addition, the reinforcement effects, influenced by the support parameters, can be reflected by rock mass displacement. In this section, the influences of the parameters, including pretension force, cross-section area, length, and support density, are analyzed, while other parameters are shown in Table 1.

5.1.1 *Pretension forces and cross-section areas of rock bolt and anchor cable*

The pretension force F_1^0 and cross-section area A_1 of rock bolt are analyzed firstly. As the pretension force F_1^0 increases, the anchoring force F_1 represents approximately a linear rising trend (actually a concave curve), in Figure 9(a), indicating that the reinforcement effects are enhanced. In addition, a larger pretension force also leads to a smaller passive anchoring force and less surplus of rock bolt strength. Apparently, the magnitude of F_1 is smaller than the yielding force of rock bolt, which indicates that there is a reasonable range of the pretension force. When F_1 exceeds

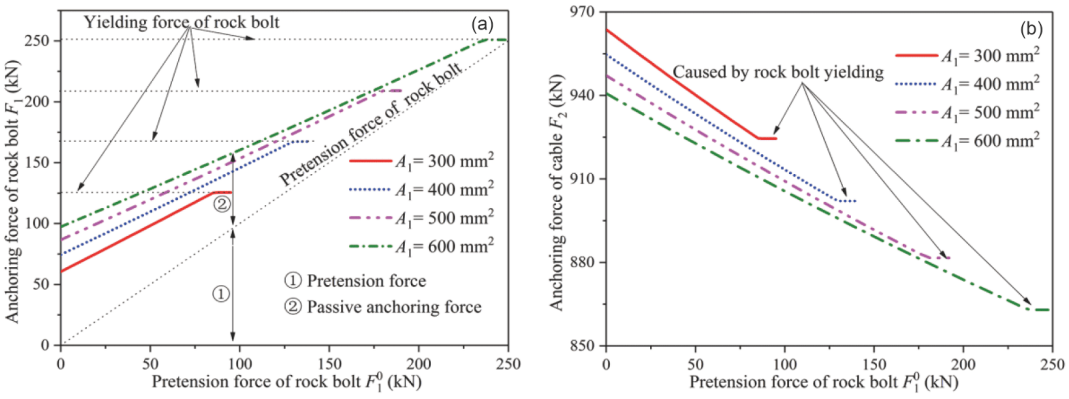

Figure 9 (Color online) Anchoring force influenced by F_1^0 and A_1. (a) Anchoring force of rock bolt F_1; (b) anchoring force of cable F_2.

this range, the rock bolt exhibits the yield behavior, which means the failure of rock bolt.

The cross-section area A_1 also plays an important role. As shown in Figure 9(a), while A_1 increases from 300 to 600 mm^2, the yielding force F_1^p increases from 125.5 to 251 kN. The increase of the cross-section area can significantly improve the bearing capacity of rock bolt, which means larger pretension force can be applied to the rock bolt. In addition, the increase of the cross-section area also improves the stiffness of the rock bolt.

As shown in Figure 9(b), the aforementioned two factors of rock bolt can affect the mechanical state of cable. With the increase of F_1^0, the cable force F_2 decreases until the yield of the rock bolt. The increase of the cross-section area A_1 also leads to slightly decrease of F_2. This phenomenon indicates that the values of pretension force F_1^0 and cross-section area A_1 can change the load-bearing ratio of the bolt-cable support. In other words, with larger values of F_1^0 and A_1, the rock bolt subjects to more load while the cable bears less load than before.

The pretension force F_2^0 and the cross-section area A_2 of cable have similar reinforcement effects as rock bolt (Figure 10): A_2 determines the bearing capacity, and F_2^0 determines the anchoring force of cable. But there is a little difference. Comparing Figure 9(a) with Figure 10(a), the passive anchoring force is a considerable part of the rock bolt force. Thus, with a small pretension force F_1^0, the anchoring force F_1 is still available to tunnel reinforcement. But it is different to cable force F_2, in which the pretension force F_2^0 has a dominant position, and the component of passive anchoring force in F_2 is small. If the cable pretension force F_2^0 is too small, its reinforcement effects on rock mass are insufficient. Then, the rock bolt has to bear more load than before, and yield failure of rock bolt may occur (Figure 10(b)). Therefore, in the bolt-cable combined support, enough pretension force should be applied on the anchor cable.

The development of u_0 (radial displacement at tunnel circumference) with different pretension forces is shown in Figure 11. The radial displacement u_0 steadily decreases with the increase of pretension forces, which means the pretension forces are helpful to rock mass reinforcement. However, there are two special zones in Figure 11(a): the rock bolt yielding zone and the cable yielding zone. When the materials reach yield strength, failure of rock bolt or anchor cable may occur. Hence, there are suitable ranges of F_1^0 and F_2^0. In these ranges, larger pretension forces contribute more to rock mass reinforcement. Comparing Figure 11(a) and (b), we can

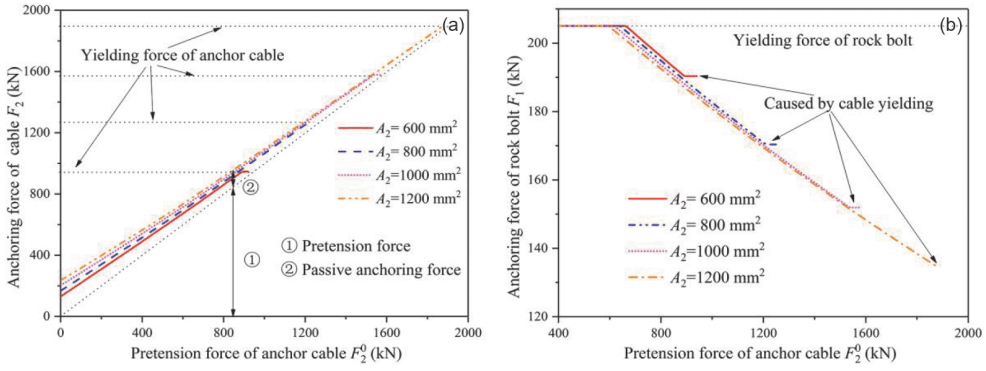

Figure 10 (Color online) Anchoring force influenced by F_2^0 and A_2. (a) Anchoring force of cable F_2; (b) anchoring force of rock bolt F_1.

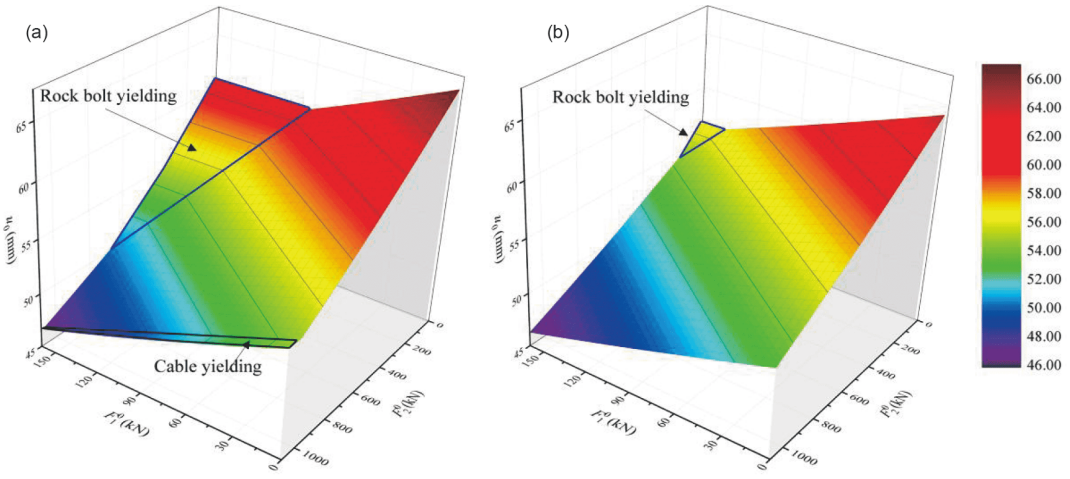

Figure 11 Displacement at tunnel circumference influenced by F_1^0, $F_2^0$and A_1, A_2. (a) Condition of A_1=500 mm^2 and A_2=800 mm^2; (b) condition of A_1=600 mm^2 and A_2=1000 mm^2.

see the radial displacement u_0 decreases slightly with the increase of cross-section areas. In addition, the cable yielding zone disappears, and the dimension of rock bolt yielding zone is greatly reduced. It reveals that the cross-section areas A_1 and A_2 determine the bearing capacity of bolt-cable support. The remaining rock bolt yielding zone also indicates that enough pretension force should be applied to the anchor cable to avoid the failure of rock bolt.

5.1.2 Lengths and supporting densities of rock bolt and anchor cable

The lengths of bolt and cable determine the reinforcement range. In the following, the discussed length is the free length as shown in Figure 1. The supporting density is the amount of supporting members per unit area. Figure 12(a) shows the relationship between the supporting density λ_1, length L_1, and displacement u_0. A higher supporting density λ_1 is helpful to improve the reinforcement on rock mass, which leads to a smaller displacement. As the curve slope gradually decreases, after the support density reaching a certain value, its influences on tunnel reinforcement will be limited. The length L_1 of rock bolt determines its reinforcement radius R_1 (R_1=R_0+L_1). In general, the rock mass deformation decreases with the increase of L_1. As shown in Figure 12(a), the mechanical state of Cases 1–3 may occur according to the length of L_1. For the cases L_1=1, 2 m, the rock bolt is anchored in the plastic residual zone. Considering the fixed cable reinforcement radius R_2=26 m, the relationship R_1<R_r<R_p<R_2 belongs to Case 1 in Figure 4(b). Such a short length of rock bolt cannot meet the requirement of tunnel reinforcement. As a result, it produces large displacement u_0. For the cases L_1=4, 5, 6, 7, 8 m, the rock bolt is anchored in the strain softening zone. The relationship R_r<R_1<R_p<R_2 belongs to Case 2. The sharp reduction of u_0 indicates that there is a notable improvement on the reinforcement effects. For the cases L_1=10, 11 m, the rock bolt is anchored in the elastic zone. It satisfies the condition R_r<R_p<R_1<R_2 that belongs to Case 3. Comparing with the results in Case 2, u_0 is slightly reduced in this situation while the rock bolt reinforced radius R_1 is approximately equal to cable reinforced radius R_2. However, considering the short-long coupling anchorage design of the bolt-cable support, the overlength

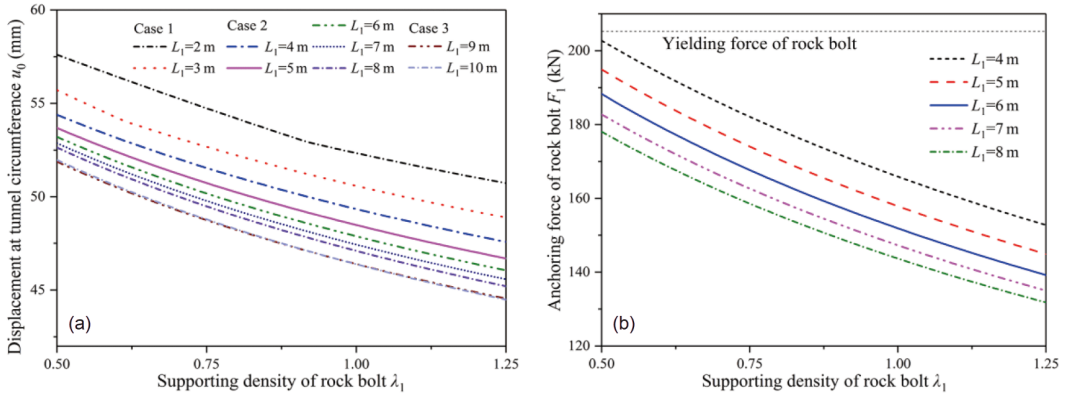

Figure 12 Influence of supporting density λ_1 and length L_1 of rock bolt. (a) On radial displacement at tunnel circumference; (b) on anchoring force of rock bolt.

rock bolt of Case 3 is unreasonable. According to the above analysis, it is suggested that the rock bolt should be anchored in the strain softening zone to provide reinforcement for the plastic residual zone.

Figure 12(b) shows the relationship of the rock bolt force F_1 with λ_1 and L_1. With the increase of λ_1 and L_1, the anchoring force F_1 is gradually reduced. With a short length of L_1=4 m and a small supporting density λ_1, the rock bolt exhibits a large anchoring force approaching the yielding force. This result indicates that small values of L_1 and λ_1 may cause failure risk of rock bolt and is unreasonable in tunnel design.

The length L_2 and supporting density λ_2 of anchor cable have similar reinforcement effects as those of the rock bolt. The advantages of anchor cable are the long reinforcement length and the high load-bearing capacity. With the distal end anchored in the deep stable rock mass, a considerable force can be produced at the head end to support the unstable rock mass around the tunnel. So, it is crucial for the cable to be anchored in stable rock mass (elastic zone). When the cable is anchored in the elastic zone, as shown in Figure 13, there is a limited improvement on rock mass reinforcement by increasing the cable length L_2. On the contrary, higher supporting density is still useful to stabilize the rock mass. In practical engineering, the installation of cables requires huge and deep holes, the drilling process of which leads to considerable disturbance for the rock mass. In addition, the cables together with their installations are expensive. Determining the value of λ_2 should consider both the cost and the reinforcement effects.

As shown in Figure 13(b), the cable force F_2 is also associated with L_2 and λ_2. For cables anchored in the elastic zone, a longer cable may lead to a smaller anchoring force, which cannot take enough advantages of the cable strength. That means the cables should not be too long in tunnel design. With a higher supporting density λ_2, the load carried by every single cable is reduced. The cable force F_2 shows a reduction trend with the increase of λ_2.

In the bolt-cable support, increasing the supporting density λ_1 and λ_2 can improve the reinforcement effects, but their values should not exceed the reasonable ranges. The lengths L_1 and L_2 should satisfy that the rock bolt is anchored in the strain softening zone and the cable is anchored in elastic zone. The above analysis shows that the analytical model is helpful in determining the parameters of the bolt-cable support.

5.2 Stress distribution of rock mass

With suitable geometric dimensions (lengths and cross-section areas) of rock bolt and anchor cable, the pretension forces and supporting densities determine the mechanical state of rock mass. Hence, the stress distributions of rock mass related to F_1^0, F_2^0, λ_1, and λ_2 are shown in Figure 14. The λ_i and F_i^0 (A_i matching with F_i^0) of different patterns and the analytical results of plastic residual radius R_r, strain softening radius R_p, and displacement u_0 are listed in Table 2, while other parameters are the same as those in Table 1.

In Figure 14, the radial stress σ_r gradually increases and tends to stabilize at the initial rock mass stress. The value of σ_θ varies according to the distance from tunnel circumference. It increases rapidly in the plastic zone (especially in the strain softening zone) until reaching the peak stress at the elastic-plastic boundary. Then it decreases in the elastic zone, and eventually tends to stabilize at the initial rock mass stress. Due to the stress release effect, there are the minimum values of σ_θ and σ_r at the tunnel circumference, while there are the maximum stress differences (σ_θ−σ_r) at the elastic-plastic boundary. At the anchoring positions of rock bolt (r=R_2) and anchor cable (r=R_2), due to the anchoring force, there are pressures $p_1'$and p_2'on the rock mass, respectively. Therefore, stress jumps can be observed at the anchoring boundaries of the bolt-cable support.

The reinforcement plays an important role in the stress distribution of rock mass. Comparing with pattern 1 in Figure 14(a), the stress curves of patterns 2 and 3 shift left. The

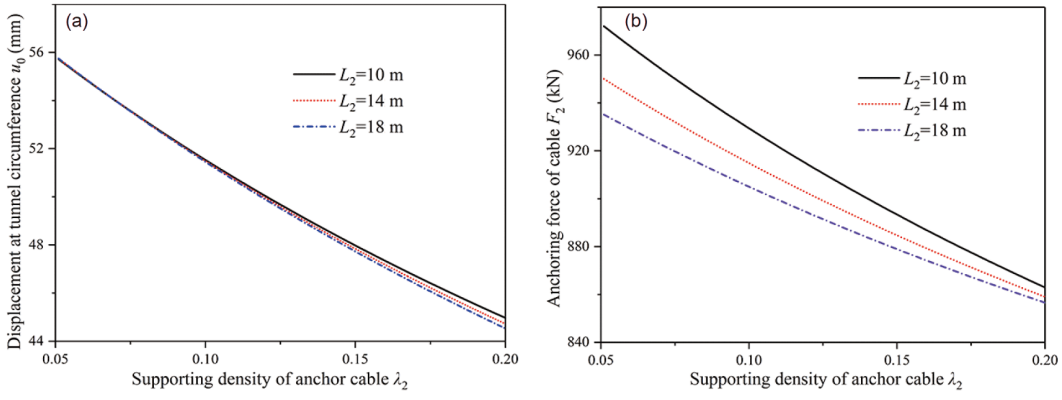

Figure 13 (Color online) Influence of supporting density λ_2 and length L_2 of anchor cable. (a) On radial displacement at tunnel circumference; (b) on anchoring force of anchor cable.

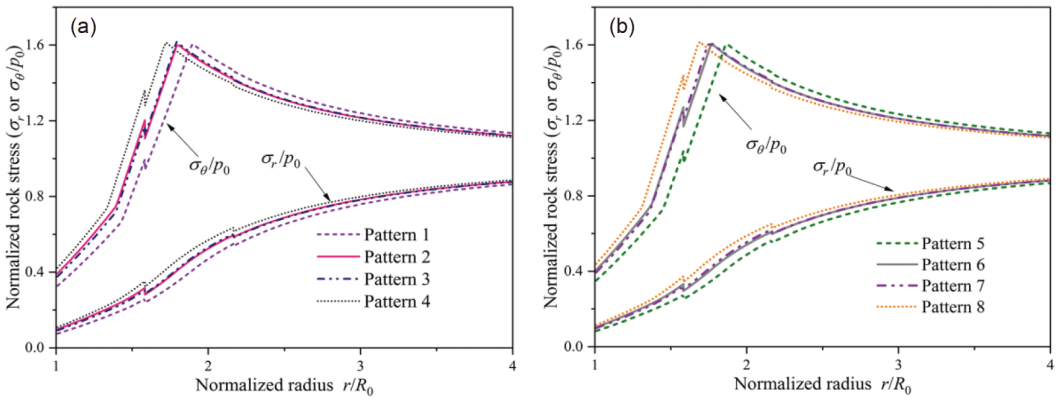

Figure 14 (Color online) Stress distribution of different patterns. (a) Patterns 1–4; (b) patterns 5–8.

Table 2 Parameters and corresponding results of different supporting patterns

No.	Parameters				R_r (m)	R_p (m)	u_0 (mm)
Pattern 1	F_1^0 = 80 kN	A_1 = 300 mm^2	F_2^0 = 500 kN	A_2 = 600 mm^2	23.46	18.24	63.25
Pattern 2	F_1^0 = 160 kN	A_1 = 600 mm^2	F_2^0 = 500 kN	A_2 = 600 mm^2	22.14	17.21	55.42
Pattern 3	F_1^0 = 80 kN	A_1 = 300 mm^2	F_2^0 = 1000 kN	A_2 = 1200 mm^2	22.06	17.16	55.30
Pattern 4	F_1^0 = 160 kN	A_1 = 600 mm^2	F_2^0 = 1000 kN	A_2 = 1200 mm^2	21.22	16.51	50.62
Pattern 5	λ_1 = 0.5		λ_2 = 0.08		22.94	17.83	60.13
Pattern 6	λ_1 = 1.0		λ_2 = 0.08		21.80	16.95	53.58
Pattern 7	λ_1 = 0.5		λ_2 = 0.16		21.59	16.80	52.78
Pattern 8	λ_1 = 1.0		λ_2 = 0.16		20.83	16.21	48.66

plastic zone radii of patterns 2 and 3 are almost the same, indicating that the pretension force F_1^0 has a similar effect as F_2^0 on stress state of rock mass. The plastic zone radius of pattern 4 is the smallest as F_1^0 and F_2^0 are increased simultaneously. Figure 14(b) shows the influences of supporting density λ_i on rock mass reinforcement. Comparing with pattern 5, R_r and R_p of patterns 6–8 have been reduced in different extents. Obviously, the reinforcement effects of the bolt-cable support are closely related to the pretension forces and supporting densities. Large pretension forces and supporting densities of bolt-cable support that can reduce the scope of plastic zone, is preferred in large cross-section tunnel design.

5.3 Ground response curve of tunnel reinforced by bolt-cable combined support

The convergence-confine curve considering the rock mass reinforcement is a useful tool for tunnel design [41–43]. The pretensioned rock bolt or anchor cable is typically considered as a part of the internal supporting systems (such as shotcrete and steel arch) rather than a component of the reinforced rock mass, and the anchoring force is considered as an internal support force [44, 45]. As shown in Figure 15, the ultimate convergence can be found at the intersection of support characteristic curve (SCC) of pretensioned rock bolt and GRC of unreinforced tunnel. However, this concept simplifies the bolting pressures p and p' that applied to both ends of the reinforced rock mass into a single internal pressure p. Such simplification cannot adequately describe the actual stress state and underestimates the anchoring effects. To address this issue, the effects of rock bolt and anchor cable are considered into the GRC in this study. The GRC of unreinforced tunnel before or without the installation of bolt-cable support can be obtained by eq. (36). The displacement solutions of Cases 1–9 are used to obtain the GRC after the installation of pretensioned rock bolt and anchor cable.

The GRCs related to pretension forces are shown in Figure 16. When no pretension force is applied ($F_1^0 = F_2^0 = 0$), the rock mass is reinforced by passive anchoring force and generates a large displacement u_0. When the pretension forces increase to $F_1^0 = 80$ kN and $F_2^0 = 500$ kN, there is a sudden drop in the GRC, which means the required internal supporting force becomes smaller due to the installation of pretensioned bolt-cable support. This drop of GRC can also

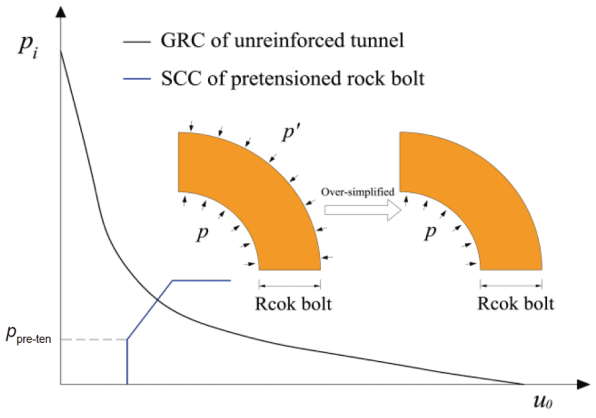

Figure 15 Traditional convergence-confine curve of tunnel reinforced by pretensioned rock bolt or anchor cable.

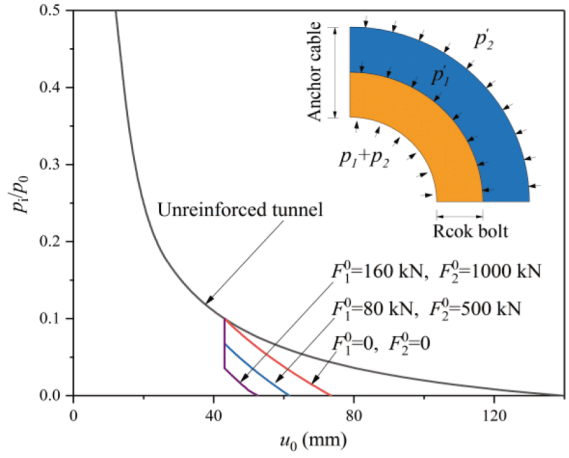

Figure 16 (Color online) GRC considering bolt-cable reinforcement with different pretension forces.

be found in a previous study of pretensioned rock bolt [18]. As a result, there is a reduction in tunnel convergence. With the increase of F_1^0 and F_2^0, the ultimate convergence tends to be smaller again, which means large pretension forces can

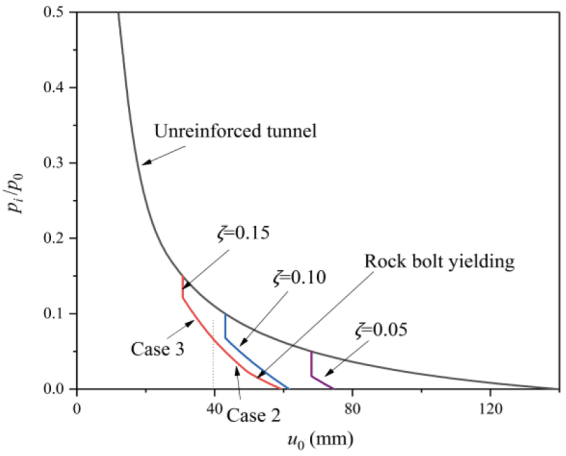

Figure 17 (Color online) GRC considering bolt-cable reinforcement with different installing time of bolt-cable support.

enhance the reinforcement effects of the bolt-cable support. The delay effect of installation can be evaluated by the stress release factor ξ, while larger ξ means the earlier installation of bolt-cable support as shown in Figure 17. As ξ increases from 0.05 to 0.15, the ultimate tunnel convergence decreases from 74.5 to 59.3 mm. It demonstrates that timely installation of bolt-cable support is crucial to rock mass reinforcement.

6 Application of proposed analytical model

In this section, we use the proposed model to study the effects of the bolt-cable support of the Great Wall Station Tunnel. This tunnel is part of the Beijing-Zhangjiakou high-speed railway, which will serve for the 2022 Beijing Winter Olympic Games. There are two super large cross-section tunnels at both ends of the station. Figure 18 shows the cross-section and geology conditions. Based on the engineering design data and geological investigation data, the mechanical parameters of rock mass, bolts, and cables are listed in

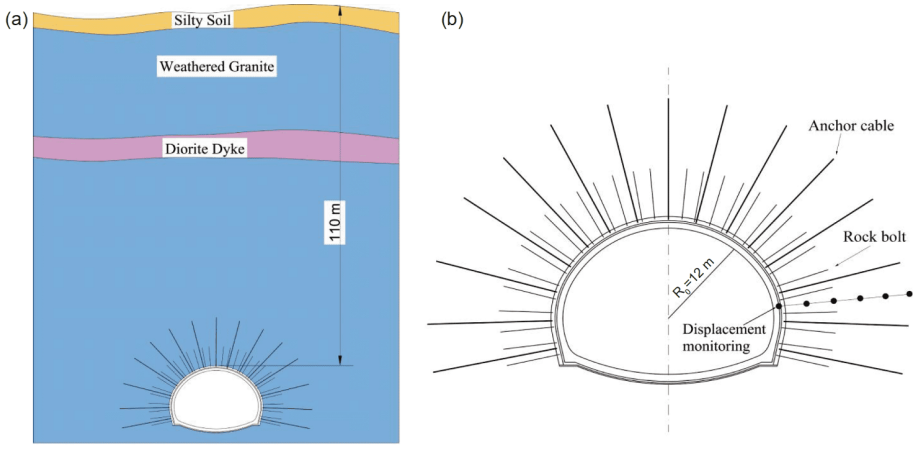

Figure 18 (Color online) Study section of Great Wall Station Tunnel in Beijing. (a) Geology conditions; (b) tunnel section and field measuring detail.

Table 1. The applicability of the proposed model can be evaluated by the comparison between the analytical solutions and the field measuring data of rock mass displacement [46].

The multi-point extensometer and total station were used for displacement monitoring of the Great Wall Station Tunnel. As shown in Figure 19, the multi-point extensometer measured the position of five anchor points relative to a reference head through the extension of rods inside sleeves, which provided the relative displacements of rock mass at the anchor points. Then, referring to the displacement at tunnel circumference monitored by the total station, the absolute displacement at the anchor points can be obtained. The multi-point extensometer instruments were installed together with the rock bolts and cables, so only the displacement u''_{r} after the installation of bolt-cable support is discussed in this section.

Substituting the mechanical parameters in Table 1 into the analytical solutions, the radii of plastic softening zone R_{p} =21.0 m and residual zone R_{r}=15.9 m, are obtained. There is the relationship $R_{\mathrm{r}}<R_1<R_{\mathrm{p}}<R_2$ that belongs to Case 2. Figure 20 shows the comparison of displacement u''_{r} of analytical results and field measuring data. The analytical results are basically consistent with the field measuring data. Therefore, it demonstrates that the proposed analytical model of the pretensioned bolt-cable combined support can provide effective information in preliminary tunnel design.

7 Conclusions

An analytical model is proposed for the design of pretensioned bolt-cable support for large cross-section tunnel. Our proposed model can consider the different mechanical cases of tunneling reinforced by the bolt-cable support. The analytical model is verified by numerical simulation. The key findings are as follows.

Large pretension forces of bolt-cable support are helpful to reduce the rock mass deformation, but the pretension forces

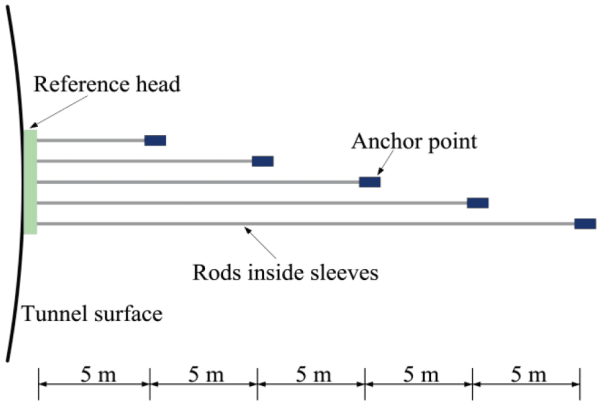

Figure 19 (Color online) The multi-point extensometer.

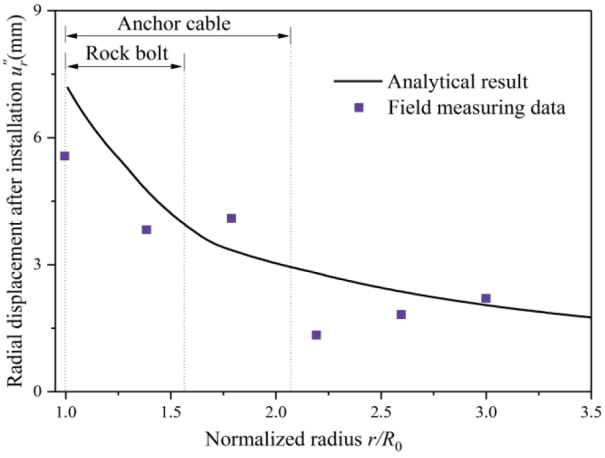

Figure 20 (Color online) Radial displacement of rock mass after installation of the bolt-cable support.

F_1^0 and F_2^0 should be suited to the cross-section areas A_1 and A_2 to avoid the yielding failure of bolt-cable support. To achieve effective coupling of rock bolt and anchor cable, the lengths L_1 and L_2 should satisfy the conditions that rock bolt is anchored in the strain softening zone and cable anchored in the elastic zone. Increasing the supporting density λ_1 and λ_2 are also helpful to improve the reinforcement effects.

A new GRC considering the reinforcement effects of pretensioned bolt-cable support is obtained, which shows the pretension forces F_1^0 and F_2^0 can effectively control rock mass deformation, and the timely installation of the bolt-cable support is also helpful to tunnel reinforcement.

The proposed model is applied to the analysis of the Great Wall Station Tunnel. The analytical results agree well with the field measuring data, which means the analytical model of the bolt-cable support is a useful tool for preliminary tunnel design.

This work was supported by the National Key Research and Development Program of China (Grant No. 2017YFC0805401), the National Natural Science Foundation of China (Grant No. 51738002), the China Railway Corporation Research and Development Program of Science and Technology (Grant No. 2014004-C), and the Fundamental Research Funds for the Central Universities (Grant No. C17JB00030).

Supporting Information

The supporting information is available online at tech.scichina.com and link.springer.com. The supporting materials are published as submitted, without typesetting or editing. The responsibility for scientific accuracy and content remains entirely with the authors.

1 Li C C. Rockbolting: Principles and Applications. Oxford: Butterworth-Heinemann, 2017
2 ovári K. History of the sprayed concrete lining method—Part II: Milestones up to the 1960s. Tunn Undergr Sp Tech, 2003, 18: 71–83
3 Hoek E, Brown E T. Underground Excavations in Rock. Boca Raton (FL): CRC Press, 1980

4 Windsor C R. Rock reinforcement systems. Int J Rock Mech Min Sci, 1997, 34: 919–951
5 Beard M D, Lowe M J S. Non-destructive testing of rock bolts using guided ultrasonic waves. Int J Rock Mech Min Sci, 2003, 40: 527–536
6 Kang H P, Wu Y, Gao F, et al. Fracture characteristics in rock bolts in underground coal mine roadways. Int J Rock Mech Min Sci, 2013, 62: 105–112
7 Li C C. Field observations of rock bolts in high stress rock masses. Rock Mech Rock Eng, 2010, 43: 491–496
8 Marenče M, Swoboda G. Numerical model for rock bolts with consideration of rock joint movements. Rock Mech Rock Engng, 1995, 28: 145–165
9 Osgoui R R, Oreste P. Convergence-control approach for rock tunnels reinforced by grouted bolts, using the homogenization concept. Geotech Geol Eng, 2007, 25: 431–440
10 Carranza-Torres C. Analytical and numerical study of the mechanics of rockbolt reinforcement around tunnels in rock masses. Rock Mech Rock Eng, 2009, 42: 175–228
11 Tan C H. Difference solution of passive bolts reinforcement around a circular opening in elastoplastic rock mass. Int J Rock Mech Min Sci, 2016, 81: 28–38
12 Yan Z X, Cai H C, Wang Q M, et al. Finite difference numerical simulation of guided wave propagation in the full grouted rock bolt. Sci China Tech Sci, 2011, 54: 1292–1299
13 Wu X Z, Jiang Y J, Guan Z C, et al. Estimating the support effect of energy-absorbing rock bolts based on the mechanical work transfer ability. Int J Rock Mech Min Sci, 2018, 103: 168–178
14 Wu X Z, Jiang Y J, Wang G, et al. Performance of a new yielding rock bolt under pull and shear loading conditions. Rock Mech Rock Eng, 2019, 52: 3401–3412
15 Pelizza S, Oreste P P, Peila D, et al. Stability analysis of a large cavern in Italy for quarrying exploitation of a pink marble. Tunn Undergr Sp Tech, 2000, 15: 421–435
16 Miura K. Design and construction of mountain tunnels in Japan. Tunn Undergr Sp Tech, 2003, 18: 115–126
17 Ranjbarnia M, Fahimifar A, Oreste P. A simplified model to study the behavior of pre-tensioned fully grouted bolts around tunnels and to analyze the more important influencing parameters. J Min Sci, 2014, 50: 533–548
18 Labiouse V. Ground response curves for rock excavations supported by ungrouted tensioned rockbolts. Rock Mech Rock Engng, 1996, 29: 19–38
19 Zhang D L, Wang M S, Gao J, et al. Construction technique of large-span tunnel under condition of complicated surrounding rock (in Chinese). Chin J Rock Mech Eng, 2003, 22: 290–296
20 Fahimifar A, Ranjbarnia M. Analytical approach for the design of active grouted rockbolts in tunnel stability based on convergence-confinement method. Tunn Undergr Sp Tech, 2009, 24: 363–375
21 Zhang X P, Wong L N Y, Wang S J, et al. Engineering properties of quartz mica schist. Eng Geol, 2011, 121: 135–149
22 Zhang X P, Wu S, Afolagboye L O, et al. Using the point load test to analyze the strength anisotropy of quartz mica schist along an exploration adit. Rock Mech Rock Eng, 2016, 49: 1967–1975
23 Gao Y, Wong L N Y, Gao F. Finite deformation analysis on sandstone subjected to thermo-hydro-mechanical (T-H-M) coupling. Rock Mech Rock Eng, 2015, 48: 159–177
24 Cheng X S, Zheng G, Soga K, et al. Post-failure behavior of tunnel heading collapse by MPM simulation. Sci China Tech Sci, 2015, 58: 2139–2152
25 Sun X M, Xu H C, He M C, et al. Thermography analyses of rock fracture due to excavation and overloading for tunnel in 30° inclined strata. Sci China Tech Sci, 2017, 60: 911–923
26 Jiang Q, Feng X T, Cui J, et al. Failure mechanism of unbonded prestressed thru-anchor cables: *In situ* investigation in large underground caverns. Rock Mech Rock Eng, 2014, 48: 873–878
27 Kang H P. Support technologies for deep and complex roadways in underground coal mines: A review. Int J Coal Sci Technol, 2014, 1: 261–277
28 Qing W, Gao Y, Zhu Y, et al. Construction methods for ultra large-span four-track deep tunnel on Wumengshan No.2 exit section. Tunn Constr, 2018, 38: 91–102
29 Shan R L, Wei Z T, Kong X S, et al. Coupled supporting of rock bolt and anchor cable in large cross-section roadway. Appl Mech Mater, 2012, 256-259: 1417–1421
30 Wang W C, Wei W B, Wang L. Numerical simulation study on combined supporting scheme of bolts and anchor cable. Appl Mech Mater, 2014, 638-640: 898–903
31 Meng Q B, Han L J, Sun J W, et al. Experimental study on the bolt-cable combined supporting technology for the extraction roadways in weakly cemented strata. Int J Min Sci Tech, 2015, 25: 113–119
32 Kang H P, Lin J, Fan M J. Investigation on support pattern of a coal mine roadway within soft rocks—A case study. Int J Coal Geol, 2015, 140: 31–40
33 Gu X, Xia Y Y, Chen A M. Variation characteristics of anchor cable prestress during underground opening excavation and overloading (in Chinese). Chin J Rock Mech Eng, 2007, 26: 4238–4244
34 Carranza-Torres C, Rysdahl B, Kasim M. On the elastic analysis of a circular lined tunnel considering the delayed installation of the support. Int J Rock Mech Min Sci, 2013, 61: 57–85
35 Cai Y, Esaki T, Jiang Y J. An analytical model to predict axial load in grouted rock bolt for soft rock tunnelling. Tunn Undergr Sp Tech, 2004, 19: 607–618
36 Möller S C. Tunnel induced settlements and structural forces in linings. Ph. D. Thesis. Stuttgart, Germany: Universität Stuttgart, 2006
37 Bobet A, Einstein H H. Tunnel reinforcement with rockbolts. Tunn Undergr Sp Tech, 2011, 26: 100–123
38 Kim S H, Pelizza S, Kim J S. A study of strength parameters in the reinforced ground by rock bolts. Tunn Undergr Sp Tech, 2006, 21: 378–379
39 Zhang G M, Li Y P, Yang C H, et al. Discussion on relationship between post-peak curves and shear strength parameters of rocks subjected to direct shear tests (in Chinese). Chin J Rock Mech Eng, 2012, 31: 2981–2988
40 Sadd M H. Elasticity: Theory, Applications, and Numerics. London: Academic Press, 2009
41 Fang Q, Zhang D L, Zhou P, et al. Ground reaction curves for deep circular tunnels considering the effect of ground reinforcement. Int J Rock Mech Min Sci, 2013, 60: 401–412
42 Carranza-Torres C, Fairhurst C. Application of the Convergence-Confinement method of tunnel design to rock masses that satisfy the Hoek-Brown failure criterion. Tunn Undergr Sp Tech, 2000, 15: 187–213
43 Li P F, Wang F, Fang Q. Undrained analysis of ground reaction curves for deep tunnels in saturated ground considering the effect of ground reinforcement. Tunn Undergr Sp Tech, 2018, 71: 579–590
44 Stille H, Holmberg M, Nord G. Support of weak rock with grouted bolts and shotcrete. Int J Rock Mech Min Sci Geomech Abstracts, 1989, 26: 99–113
45 Ranjbarnia M, Fahimifar A, Oreste P. Practical method for the design of pretensioned fully grouted rockbolts in tunnels. Int J Geomech, 2015, 16: 04015012
46 Zhang Z G, Huang M S, Xi X G, et al. Complex variable solutions for soil and liner deformation due to tunneling in clays. Int J Geomech, 2018, 18: 04018074